Computational Study of the HCCO + NO Reaction: ab Initio MO/vRRKM Calculations of the Total Rate Constant and Product Branching Ratios

I. V. Tokmakov, L. V. Moskaleva,† D. V. Paschenko, and M. C. Lin*

Department of Chemistry, Emory University, Atlanta, Georgia 30322

Received: September 9, 2002

Accurate thermochemistry for major product channels of the HCCO + NO (R1) reaction was established at the CCSD(T)/6-311+G(3df,2p) and QCISD(T)/6-311+G(3df,2p) levels of theory based on the potential energy surface (PES) calculated by density functional B3LYP/6-311G(d,p) method. Two barrierless entrance pathways forming *trans*- and *cis*-nitrosoketene (**1** and **2**) have been mapped out following the minimum energy paths. Using isodesmic reaction analysis, the standard enthalpy of formation for **1** is found to be 17.8 ± 1.7 kcal/mol. The recently reported PES of the nitrosoketene decomposition (Vereecken, L.; Sumathy, R.; Carl, S. A.; Peeters, *J. Chem. Phys. Lett.* **2001**, *344*, 400) has been appended with two additional pathways to form HCNO + CO (R1a) and HCN + CO_2 (R1b) products. A lower-energetic transition state for the decomposition of **2** to HCNO + CO has been found, and a new stepwise pathway for the decomposition of 1,2-oxazet-4-one (**3**) to HCN + CO_2 has been considered in competition with a more favorable concerted pathway. The effective total rate constant and products distribution have been calculated in the framework of multichannel and multiquantum well kinetic model, and the effects of *P* and *T* have been evaluated by weak collision master equation/RRKM approach with a variational treatment of the entrance channels. Our predicted total rate constant, $k_{R1}(T) = 1.37 \times 10^{16}\ T^{-0.98} \exp(-190/T)$ cm^3 mol^{-1} s^{-1}, exhibits a negative temperature dependence in very good agreement with experiment. The α(R1b) branching fraction can be given by $0.5 \exp(-T/67.1) + 0.3 \exp(-T/2592)$ in the 250−2500 K temperature range, which is also well-supported by available experimental data.

Introduction

Reduced NO_x emissions is an important requirement for modern technologies of hydrocarbon combustion. To date, some of the most efficient and universal solutions in the design of industrial combustion sources rely on fuel reburning technologies.[1−3] Innovative methods, such as fuel flexible reburning,[4] have been actively developed and optimized. The ketenyl radical (HCCO) is one of the free radicals responsible for NO removal in the reburning processes.[5,6] In recent experimental and kinetic modeling of plug-flow reactor[7−9] and jet-stirred reactor combustion,[10−12] the HCCO + NO recombination reaction (R1) was identified as the critical NO removal step

$$\mathrm{HCCO + NO \rightarrow products} \qquad \text{(R1)}$$

Understanding of the exact mechanism, by which reaction (R1) acts in NO scavenging, is important for optimizing the efficiency of reburning technologies.

Since the first measurement of the total rate constant by Unfried and co-workers[13] in 1991, this reaction has been investigated several times for its total rate and/or product distribution.[14−19] Unfried et al.[13] used the 193 nm excimer laser photolysis of ketene to generate the HCCO radical and IR diode laser absorption spectroscopy to detect it. Following the HCCO decay in the excess of NO, they determined the room *T* value of the total rate constant $k_{R1}(298\ \mathrm{K}) = 2.3 \times 10^{13}$ cm^3 s^{-1} molecule^{-1}. In the experiments of Temps et al.,[14] HCCO was produced in the O + C_2H_2 reaction and monitored by far-infrared laser magnetic resonance spectroscopy. For reaction with NO, they found $k_{R1}(296\ \mathrm{K}) = 1.3 \times 10^{13}$ cm^3 s^{-1} molecule^{-1}. In 1994, Boullart et al.[5] investigated the kinetics of the HCCO + NO reaction in a similar C_2H_2/O/NO system over an extended temperature range, 290−670 K, with discharge flow and molecular beam mass spectrometry techniques (D-F/MBMS). They determined the total rate coefficient, $k_{R1}(T) = (1.0 \pm 0.3) \times 10^{-10} \exp(-350 \pm 150\ \mathrm{K}/T)$ cm^3 s^{-1} molecule^{-1}, relative to the known rate coefficient of the HCCO + O reaction. According to this expression, the k_{R1} coefficient exhibited a slight positive temperature dependence within relatively large error limits. Very recently the same group measured more accurate absolute values of k_{R1} at temperatures from 297 to 802 K using a laser-photofragment/laser-induced fluorescence technique.[15] The updated k_{R1} rate coefficient was found to have a negative temperature dependence, $k_{R1}(T) = (1.6 \pm 0.2) \times 10^{-11} \exp(340 \pm 30\ \mathrm{K}/T)$ cm^3 s^{-1} molecule^{-1}.

Several product channels have been proposed for reaction (R1):[14]

$$\mathrm{HCCO + NO \rightarrow HCNO + CO} \qquad \text{(R1a)}$$
$$\mathrm{\rightarrow HCN + CO_2} \qquad \text{(R1b)}$$
$$\mathrm{\rightarrow HONC + CO} \qquad \text{(R1c)}$$
$$\mathrm{\rightarrow HNCO + CO} \qquad \text{(R1d)}$$
$$\mathrm{\rightarrow HNC + CO_2} \qquad \text{(R1e)}$$
$$\mathrm{\rightarrow HOCN + CO} \qquad \text{(R1f)}$$
$$\mathrm{\rightarrow NCO + HCO} \qquad \text{(R1g)}$$

* To whom correspondence should be addressed. E-mail: chemmcl@emory.edu. Fax: 1-404-727-6586.

† Current address: Institut für Physicalische und Theoretische Chemie, Technische Universität München, 85747 Garching, Germany.

10.1021/jp022024t CCC: $25.00
Published on Web 01/24/2003

The product distribution of the HCCO + NO reaction was first determined in the D-F/MBMS studies of the C_2H_2/O/NO system by Peeters and co-workers.[5,16] They concluded that the two main product channels were (CHN) + CO_2 and (CHNO) + CO, whereas it was not exactly clear from the mass spectroscopic characterization which of the (CHNO) and (CHN) isomers were formed as the coproducts of CO and CO_2. FTIR study by Eickhoff and Temps[17] clarified this issue by demonstrating that the coproduct of CO was HCNO rather than the thermodynamically more stable HNCO isomer. In the subsequent studies,[18,19] an agreement has been reached that the two main product channels are (R1a) and (R1b). The branching fractions for reaction (R1b) determined in ref 17 and 18 at room temperature are 0.28 ± 0.10 and 0.12 ± 0.04, respectively, whereas at 550 and 700 K, the values of 0.20 ± 0.04[16] and 0.23 ± 0.09[5] have been deduced.

The potential energy surface of reaction (R1) was first investigated by Nguyen et al.[20] in 1992 and more recently by Vereecken et al.[21] The latter theoretical study computed product branching fractions in good agreement with the experimental observations, while in strong disagreement with earlier statistical−theoretical predictions of Miller et al.,[9] who used the quantum chemical results from ref 20 and predicted an almost equal conversion of NO to HCNO (via R1a) and HCN (via R1b) at 700 K, and an even higher yield of HCN at room temperature: $k_{R1b}/k_{R1}(298\ K) = 0.82$.

Because of the complexity associated with the required variational treatment of the two entrance channels, no attempt was made to calculate the total rate constant in the previous theoretical studies. The main target of the present work was an accurate description of the entrance channels using canonical variational transition state theory (VTST) and multichannel RRKM-master equation analysis. Both entrance channels were coupled with isomerization and decomposition channels; this allowed us to derive the effective total rate constant as well as branching of the main product channels.

In the next sections, a description of the theoretical approach will be given followed by a discussion of the refined potential energy surface (PES) for the HCCO + NO reaction. Then effective rate constants and product distributions calculated by statistical theories will be analyzed with respect to experimental data. Finally, kinetic implications of our findings to combustion modeling will be discussed.

Computational Methods

Quantum chemical calculations were done with the Gaussian 98[22] suite of programs. We employed a hybrid density functional B3LYP (Becke 3-parameter hybrid exchange functional[23] combined with the LYP exchange-correlation functional[24]) with the standard 6-311G(d,p) basis set for the full geometry optimizations of the reactants, products, intermediates, and transition states. To ensure the accuracy of the electronic wave function, its stability was routinely tested, and the wave function was reoptimized whenever internal instabilities were found. The optimized equilibrium geometries of all stationary points located on the reaction potential energy surface (PES) are summarized in Figure 1. Harmonic vibrational frequencies calculated at the same level of theory were used for characterization of the stationary points as minima or saddle points and for ZPE corrections. Intrinsic reaction coordinate (IRC) calculations[25] allowed us to make unambiguous connections between the stationary points located along the reaction paths.

Our choice of the B3LYP density functional was motivated by its good performance for the geometry optimizations and

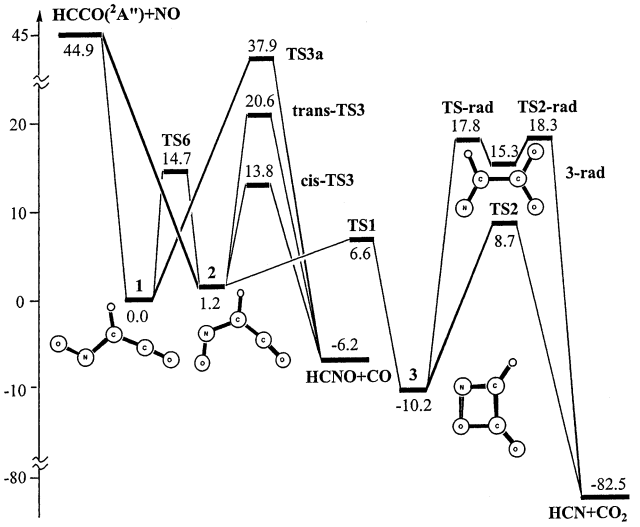

Figure 1. Schematic potential energy surface of the HCCO($^2A''$) + NO($^2\Pi$) reaction. Relative energies (kcal/mol) were taken as an average of the CCSD(T)/(II) and QCISD(T)/(II) values and include a ZPE correction calculated by the B3LYP/(I) method.

accurate prediction of vibrational frequencies.[26] Another important reason is that B3LYP can implicitly include electron correlation[27] which makes it useful for optimization of the HCCO + NO recombination profiles, where the system has partially diradical character at large intermolecular separations.

To obtain chemically accurate reaction enthalpies and barrier heights, we performed the CCSD(T) and QCISD(T) single-point calculations at the 6-311+G(3df,2p) level for the present 5 heavy atom system. Therefore, the highest levels of theory attained in this study can be denoted as CCSD(T)/(II)//B3LYP/(I) and QCISD(T)/(II)//B3LYP/(I), where we have introduced the following short notations for the basis sets: (I) for 6-311G-(d,p); (II) for 6-311+G(3df,2p).

In an attempt to calculate a more reliable enthalpy for the initial association step, an isodesmic reaction analysis was performed at various levels of theory, including CCSD(T), QCISD(T), as well as MPn, where $n = 1-4$ ($n = 1$ corresponds to HF theory) with the large 6-311+G(3df,2p) basis set.

Results and Discussion

HCCO Radical. As indicated in earlier theoretical[20,28−36] and experimental[13,37−43] studies, the ketenyl radical is a Renner-Teller species. The rotational spectrum of HCCO was observed by Endo and co-workers[38,39] who reported a bent quasilinear structure of the ground electronic state and $^2A''$ symmetry. Their work also pointed to noticeable perturbation effects owing to the presence of a low-lying Renner-Teller component, $^2A'$.

The geometry of the HCCO radical computed at the B3LYP/6-311G(d,p) level of theory can be compared with the results of the previous high level theoretical calculations and with that inferred from the microwave spectra (see Table 1). Experimentally, unfortunately, it was not possible to unambiguously determine all geometrical parameters without introducing certain assumptions, such as fixing the CCO angle at 180° and CO bond length at 1.150 Å (taken from early ab initio calculations). Under these assumptions, the HCC angle was determined to be 138.7°, some 10° larger than those predicted at the highest levels of theory considered. The B3LYP/6-311G(d,p) level employed in this work for geometry optimizations predicted the geometry of HCCO very close to that computed by Schäfer et al.[34] at the CASSCF/DZP level and differs from the CCSD(T) geometries

TABLE 1: HCCO(^{2}A″) Equilibrium Geometry and Renner-Teller Splitting: Present Level of Theory vs Experiment

method	B3LYP (this work)	CASSCF (ref 34)	CCSD(T) (ref 33)		
basis	6-311G(d,p) = (I)	DZP	PVTZ	TZ2P	expt
A, cm^{-1}	42.48		34.99	29.35	41.46[a]
B, cm^{-1}	0.364		0.364	0.363	0.363[a]
C, cm^{-1}	0.361		0.360	0.358	0.359[a]
r(C−H), Å	1.077	1.079	1.066	1.073	1.056(4)[a]
r(C−C), Å	1.318	1.322	1.297	1.310	1.314(25)[a]
r(C−O), Å	1.171	1.171	1.173	1.176	1.150[a,b]
∠HCC, deg	127.3	128.3	134.6	130.2	138.7(14)[a]
∠CCO, deg	169.8	163.6	169.4	168.2	180[a,b]
fundamentals, cm^{-1}:					
CH stretch	3355		3371	3324	
CCO stretch (asymm)	2092		2099	2054	2023[c]
CCO stretch (symm)	1269		1249	1210	
CCO bend (a′)	564		568	612	
torsion (a″)	508			539	
CCH bend (a′)	441		511	528	494[d]
splitting (ΔE), cm^{-1}	1140[e]	1609	643	1096	1175[f]

[a] Reference 38. [b] Fixed. [c] Reference 13. [d] Reference 42. [e] Calculated at the CCSD(T)/(II)//B3LYP/(I) level, ΔE(B3LYP/(I)) = 331 cm^{-1}. [f] Calculated based on the formula:[38] $\epsilon_{aa} = -4A\,A_{SO}/\Delta E$, where the rotational constant A and the spin−orbit rotational constant ϵ_{aa} were experimentally determined in ref 38 and the spin−orbit splitting A_{SO} was theoretically calculated in ref 36.

by at most 6% in bond angles and 2% in bond lengths. The rotational constants, calculated at the B3LYP level, agree with experimentally measured values within experimental uncertainties.

The theoretically predicted harmonic vibrational frequencies computed at the B3LYP/6-311G(d,p) level of theory are in very good agreement with earlier high level calculations. Experimentally, only ν_2 and ν_6 were measured.[13,40−42] These ground-state fundamentals agree very well with our values computed at the B3LYP/6-311G(d,p) level.

Another important parameter which can be compared with experiment and other MO calculations is the Renner-Teller splitting (ΔE), i.e., the energy difference of the 1^2A′($1^2\Pi$) and ^{2}A″($1^2\Pi$) equilibrium geometries. As demonstrated by previous theoretical investigations, this quantity is very sensitive to the method and basis set employed (some of the best levels of theory are summarized in Table 1). It is seen from Table 1 that the CCSD(T)/(II) and QCISD(T)/(II) predictions, 1140 and 1136 cm^{-1}, are in excellent agreement with ΔE = 1175 cm^{-1} inferred from the experimental spin−rotational constant[38] and theoretically predicted[36] spin−orbit splitting in the ground state of HCCO (see footnotes of Table 1). The B3LYP value, 331 cm^{-1}, is apparently too small.

HCCO + NO Potential Energy Surface. The potential energy surface of the title reaction was investigated earlier by Nguyen et al.[20] at the QCISD(T)/6-311G(d,p)//HF/6-31G(d,p) level and more recently by Vereecken et al.[21] at the CCSD(T)/6-311+G(2d,p)//B3LYP-6-311++G(d,p) and CCSD(T)/6-311+G(2d,p)//CCSD(T)/6-31G(d,p) levels. Plausible pathways for channels (R1a), (R1b), and (R1c) were mapped out step by step; a branch leading to the HNCO + CO products (R1d) was also considered, but its connection to the reactants could not be found.

In the present work, we examined the main accessible channels (R1a and R1b) and unveiled important pathways overlooked in the previous studies. The energetics have been refined by single-point calculations at the CCSD(T)/(II) and QCISD(T)/(II) levels, where (II) stands for the large 6-311+G-(3df,2p) basis set. Updated potential energy profiles are shown in Figure 1. The equilibrium geometries of the intermediates and transition states are shown in Figure 2. We have also computed one-dimensional reaction profiles for the two barrierless entrance channels to form two initial adducts, *cis*- and *trans*-nitrosoketene, denoted as **1** and **2**, respectively. The initial addition steps will be discussed in more detail in the section devoted to variational calculations.

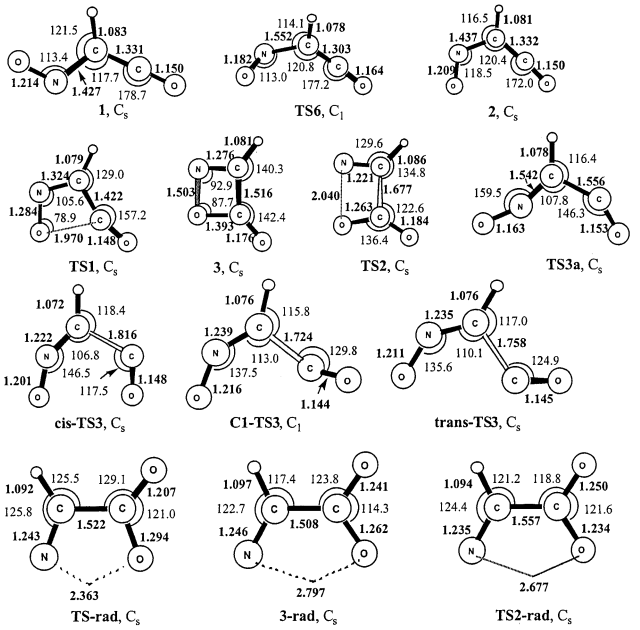

Figure 2. Molecular structures of intermediates and transition states fully optimized at the B3LYP/6-311G(d,p) level of theory.

We will now briefly comment on the most important features of the PES (see Figure 1). In the first theoretical study of this reaction, Nguyen et al.[20] did not look for the transition state connecting cis and trans isomers **1** and **2**. It was assumed that the barrier for internal rotation around the single C−N bond is small, and the isomers can easily interchange. In fact, the C−N bond in nitrosoketene has a significant π character because of delocalization of the π-electronic density over conjugated C=C and N=O double bonds. Consequently, the rotational barrier in nitrosoketene is high. In the recent studies of Badawi and Forner[44] and Vereecken et al.,[21] its value relative to **1** was estimated to be 18 and 14 kcal/mol, respectively. Our prediction of 14.7 kcal/mol (see Figure 1 and Table 2) is in agreement with these estimates. An important implication of the relatively

TABLE 2: Energetics (kcal/mol) of the Nitrosoketene Decomposition

species/TS	B3LYP/(I)	CCSD(T)/(II)// B3LYP/(I)	QCISD(T)/(II)// B3LYP/(I)	Nguyen et al.[a]	Vereecken et al.[b]
1	0.00	0.00	0.00	0.0	0.0
2	1.09	1.28	1.12	1.5	1.4
3	−2.44	−10.28	−10.17	−7.5	−9.0
3-rad[c]	13.07	15.64	14.98	(−)	(−)
TS1	8.57	6.90	6.27	8.0	6.7
TS2	12.43	9.71	7.74	13.8	8.1
cis-TS3	16.47	13.94	13.63	(−)	(−)
trans-TS3	23.91	20.98	20.21	26.5	19.6
TS3a	37.57	39.20	36.54	(−)	(19.6)[d]
TS-rad[c]	13.94	18.30	17.35	(−)	(−)
TS2-rad[c]	12.68	17.52	19.06	(−)	(−)
HCN + CO_2	−77.89	−82.54	−82.46	−86.3	−84.0
HCNO + CO	−1.85	−5.66	−5.82	−7.4	−8.1

[a] QCISD(T)/(I)//HF/6-31G(d,p), ref 20. [b] CCSD(T)/6-311++G(2d,p)//B3LYP/6-311++G(d,p), ref 21. [c] Unrestricted wave functions were used in ab initio and DFT calculations for this singlet species/TS. [d] Assumed to be the same as **trans-TS3**.

high barrier of NO rotation in nitrosoketene is that its cis and trans forms have to be considered as separate intermediates in the statistical theory calculations, having their own decomposition pathways back to the reactants or to the products, which will be discussed next.

From both **1** and **2**, the extrusion of the terminal CO group can produce fulminic acid (HCNO) in a single step but in more than one way. Because the CCO fragment becomes strongly nonlinear as CO departs from either **1** or **2**, different possibilities of CO loss arise. For instance, two conformations of **TS3** connect **2** to HCNO + CO: **cis-TS3** has CO and CN bonds in a cis orientation, whereas in **trans-TS3**, the CO group is bent away from the CNO moiety. As follows from the energetics listed in Table 2, the cis orientation of the leaving CO group is energetically more favorable by ∼6−7 kcal/mol. The earlier study of Vereecken et al.[21] reported only the trans conformation of **TS3**, thus missing the more favorable CO-extrusion pathway via **cis-TS3**. However, they emphasized the importance of treating internal rotation of the leaving CO group as free in order to obtain reasonable kinetic results. The latter assumption is not well-justified, because we found that a considerable barrier of 8.8 kcal/mol separates cis and trans conformations of **TS3**. This value was taken as a difference between the energies of **cis-TS3** and a nonplanar second-order saddle-point, here denoted as **C1-TS3** (see Figure 2), which can be regarded as a barrier of internal rotation in **TS3**. Because of the relatively high magnitude of this barrier, cis and trans pathways of CO extrusion from **2** have been taken into account explicitly in this study.

Vereecken et al.[21] could not find a separate transition state connecting **1** and HCNO + CO probably because they assumed a trans orientation of the CO and CN bonds such as in **trans-TS3**; therefore, they concluded that the dissociation pathways from **1** and **2** were passing through the same transition state, **trans-TS3**, because of a facile rotation of the NO group. We, however, have found another transition state denoted as **TS3a** from **1** to HCNO + CO, with the cis configuration of the NCCO fragment, similarly to **cis-TS3. TS3a** lies more than 20 kcal/mol higher than **cis-TS3**, suggesting that the barrier for internal rotation of the NO group in **TS3** should be high. As mentioned above, the NO rotation around CN bond in nitrosoketene is hindered by ∼14.7 kcal/mol. In **TS3** (both cis and trans), the CN bond shortens as its order increases to double. Therefore, the internal rotation of the NO group in **TS3** is expected to become even more hindered, contradictory to the assumption that **1** can be directly connected to either **cis-TS3** or **trans-TS3** by virtue of "a smooth rotation of the NO group".[21] Upon closer examination, we noticed that **TS3a** corresponds to **TSpsrot** in ref 21, where it was misinterpreted as a transition state for isomerization between **1** and **2**.

In competition with (R1a), thermodynamically more favorable products, HCN + CO_2, can be formed. Earlier studies[20,21] established a pathway to these products involving **TS1**, relatively stable 1,2-oxazet-4-one (**3**) and **TS2**. The corresponding elementary steps can be described as 1,4-electrocyclization of **2**, which yields a cyclic intermediate **3**, followed by its [2+2] cycloreversion via a concerted **TS2**. The last transformation has a relatively high barrier, in accordance with Woodward−Hoffmann orbital symmetry rules.[45] In addition to this known pathway, we have also examined a stepwise dissociation of **3**, involving a diradical open-chain intermediate **3-rad**. This intermediate can be formed upon a ring-opening of **3** by breaking the NO bond (**TS-rad**) and can then dissociate to HCN + CO_2 via **TS2-rad**.

Accurate description of the stepwise pathway of 1,2-oxazet-4-one decomposition cannot be achieved without accounting for both dynamic and nondynamic correlation effects in the **TS-rad**, **3-rad**, and **TS2-rad**, all of which possess a strong diradical character, combined with a considerable degree of electron delocalization because of the interaction of nonbonding electron pairs with conjugated π bonds. In such cases, as a result of the neglect of electronic correlation, single-reference HF-based methods typically overestimate relative energies of the transition structures and intermediates involved in homolytic ring-opening reactions. A good prescription would be to use a multireference method with a sufficiently large basis set. However, we are still too limited in computational power to embark on a systematic investigation of such a high level for the present five heavy atom system.

Recently, nonlocal unrestricted DFT was successfully employed to study systems with strong effects of nondynamical electron correlation in general and homolytic ring-opening reactions in particular.[46−49] Interestingly, pure DFT methods tend to overestimate the stability of diradical transition structures and intermediates because of the inclusion of electron correlation during the optimization of the Kohn−Sham orbitals.[49] This deficiency of the pure DFT methods can be partially cured by inclusion of some HF exchange (recall that HF theory underestimates the stability of diradical species). The B3LYP is an example of hybrid functionals that include a well-balanced admixture of HF-exchange. Goddard et al.[49] applied this functional to study the ring-opening reaction of 1,2-dioxetene and obtained the energetics and geometries that were in agreement with multireference results and experimental data.

TABLE 3: Thermochemical Parameters of Selected Molecules and Radicals Relevant to This Study

species	g_i[a]	$\Delta_f H°_0$, kcal mol^{-1}	$S°_{298}$, cal mol^{-1} K^{-1}	$\Delta_f H°_{298}$, kcal mol^{-1}	ref
ketenyl (HCCO) $^2A''$	2	42.2 ± 0.7	58.8	42.2 ± 0.7	43
nitrogen oxide (NO)[b] $^2\Pi_{1/2}$	2	21.46 ± 0.04	50.4	21.58 ± 0.04	53
$^2\Pi_{3/2}$	2				
carbon monoxide (CO)	1	-27.20 ± 0.05	47.2	-26.42 ± 0.05	53
carbon dioxide (CO_2)	1	-93.97	51.2	-94.05	53
hydrogen cyanide (HCN)	1	31.9 ± 0.5	48.2	31.8 ± 2.0	74
fulminic acid (HCNO)	1	41.6 ± 2.0	56.7	41.3 ± 2.0	74
ethylene (c_2h_4)	1	14.6 ± 0.1	52.4	12.5 ± 0.1	53
trans-nitrosoethylene (C_2H_3NO)	1	43.3 ± 1.5	65.8	40.9 ± 1.5	54
ketene (CH_2CO)	1	-12.0 ± 0.1	57.7	-12.8 ± 0.1	55
trans-nitrosoketene (1)	1	18.8 ± 1.7	70.0	17.8 ± 1.7	this work

[a] Electronic degeneracy. [b] The ground state of NO radical is split into two spin−orbit components ($^2\Pi_{1/2}$ and $^2\Pi_{3/2}$, $\Delta = 121$ cm^{-1}).

TABLE 4: Enthalpy of Formation of *trans*-Nitrosoketene (1) and Heat of Reaction R1t[a]

computational methods[b]	$\Delta H°_{R2}(0\ K)$	$\Delta_f H°_0(\mathbf{1})$[c]	$\Delta H°_{R1t}(0\ K)$[d]	$\Delta H°_{R1t}(0\ K)$[e]
B3LYP/(I)	−1.2	17.9	−45.7	−42.0
MP2/(I)	−1.8	18.5	−45.1	−48.9
MP4/(I)	−1.4	18.1	−45.6	−44.7
CCSD(T)/(I)	−2.2	18.9	−44.8	−40.4
MP2/6-311+G(d,p)	−1.5	18.2	−45.4	−50.6
MP4/6-311+G(d,p)	−1.0	17.7	−46.0	−46.5
MP2/6-311G(2df,p)	−2.1	18.8	−44.8	−51.5
MP4/6-311G(2df,p)	−1.7	18.4	−45.3	−47.2
HF/(II)	−4.1	20.8	−42.9	−15.5
MP2/(II)	−2.0	18.7	−45.0	−53.0
MP3/(II)	−3.4	20.1	−43.6	−44.8
MP4/(II)	−1.5	18.2	−45.5	−48.7
QCISD(T)/(II)	−1.9	18.6	−45.0	−44.2
CCSD(T)/(II)	−2.2	18.9	−44.8	−44.4

[a] All energies are in kcal/mol and include a ZPE correction calculated at the B3LYP/(I) level of theory. [b] (I) stands for 6-311G(d,p), and (II) stands for 6-311+G(3df,2p). [c] The 0 K heats of formation of **1** are calculated from $\Delta H°_{R2}(0K)$ using eq 1. [d] Based on isodesmic $\Delta_f H°_0(\mathbf{1})$ and experimental $\Delta_f H°_0$(NO), $\Delta_f H°_0$(HCCO) from Table 3. [e] Calculated directly.

B3LYP studies of the ring-opening of some other four-member heterocyclic systems have also been reported.[48,49]

The ring-opening of **3** belongs to the same class of reactions. Not surprisingly, we obtained very reasonable structures for the ring-opening transition state **TS-rad**, intermediate diradical **3-rad**, and decomposition transition state **TS2-rad** with the unrestricted B3LYP method (see Figure 2). Although both transition states are close to **3-rad**, particularly **TS2-rad**, the corresponding imaginary vibrational frequencies (Table 6) are very different (212*i* cm^{-1} for **TS-rad** and 1194*i* cm^{-1} for **TS2-rad**). The lowest frequency of **3-rad** corresponds to the torsional motion around the single C−C bond. Despite inherent difficulties in geometry optimization on the very flat PES surrounding **3-rad**, we were also able to locate the transition state for internal rotation in this diradical. The corresponding barrier amounted to 2.7 kcal/mol, which is higher than either **TS-rad** or **TS2-rad**. In fact, the intermediate diradical **3-rad** appears as a shoulder between **TS-rad** and **TS2-rad**, so that the initial breaking of the NO bond is the most costly step in the stepwise dissociation of **3**.

As we did for all other singlet species, we tried to refine the energetics of the diradical decomposition branch by restricted CCSD(T) and QCISD(T) theories but failed to obtain meaningful results from neither coupled cluster nor quadratic CI calculations based on the RHF wave function, because it did not represent a stable solution of the HF equation for **TS-rad**, **3-rad**, and **TS2-rad**. Therefore, we carried out CCSD(T)/(II) and QCISD(T)/(II) calculations based on the stable UHF wave function for these species. Refined energetics of the diradical branch (see Table 2) qualitatively agrees with the UB3LYP/(I) predictions, but the main differences are (1) slightly increased relative energies of all 3 stationary points and (2) a slightly deeper well associated with the **3-rad** minimum. For generality, we adopted the average of CCSD(T) and QCISD(T) energies for rate constant calculations (Figure 1). However, one should bear in mind that the reliability of the CCSD(T)/(II) and QCISD-(T)/(II) energetic parameters for **TS-rad**, **3-rad**, and **TS2-rad** is lower than that for closed-shell species involved in the competing decomposition pathways. Furthermore, CCSD(T) and QCISD(T) methods probably give the upper bounds of the accurate relative energies for **TS-rad**, **3-rad**, and **TS2-rad,** because these methods cannot fully recover the nondynamical component of electron correlation.

In summary, three new pathways were added to the PES of Vereecken et al.:[21] extrusion of CO from **1** via **TS3a** (instead of **trans-TS3**), dissociation of **2** via **cis-TS3**, and a stepwise ring-opening/dissociation of **3** to HCN+CO_2. The latter two pathways have relatively low energies and were included in the model used for rate constant calculations.

We note in passing that predicted thermochemistry of the product channels is in very good agreement with the known heats of formation of HCCO, NO, HCN, and HCNO. The calculated 0 K enthalpies for reactions (R1a) and (R1b) are −50.0 and −126.7 kcal/mol at the QCISD(T)/(II) level and −49.9 and −126.9 kcal/mol at the CCSD(T)/(II) level, whereas from the experimental heats of formation (Table 3), we obtain -49.3 ± 2.8 and -125.7 ± 1.3 kcal/mol.

Finally, we want to mention many similarities of the current PES to the previously studied PES of the isoelectronic NCO + NO reaction[50] which is important for the RAPRENOx (rapid reduction of nitrogen oxides) process.[51] For the latter system, the two main accessible pathways were identified as a direct decomposition of *cis*-OCNNO to N_2O + CO and a cyclization process to form *c*-OC(O)NN− (an analogue of intermediate **3** in the present study) followed by its decomposition to N_2 + CO_2. Similarly to the HCCO + NO case, the CO_2-producing pathway was found to be energetically slightly more favorable than the one associated with CO formation. Unfortunately, the previously reported PES for the NCO + NO reaction appears to be incomplete, because it does not include the analogue of **TS6** for internal rotation of NO in OCNNO and a pathway from *cis*-OCNNO to N_2O + CO via the cis form of the CO-extrusion transition state, analogous to **cis-TS3** in this work. Although stepwise dissociation of the cyclic intermediate *c*-OC(O)NN− was not considered in the theoretical analysis of the NCO + NO reaction, this pathway would not affect the product distribution because the concerted process is already found to be so facile that *c*-OC(O)NN− once formed immediately

TABLE 5: Moments of Inertia, Symmetry Numbers (*n*), and Vibrational Frequencies[a] of the Reactants and Products

molecule	moments of inertia, I_A, I_B, $I_C/10^{-40}$ g cm^2	vibrational frequencies: symm	vibrational frequencies: ν/cm^{-1}
HCCO (^{2}A″),	0.659, 76.90, 77.54	A′	441 (494)[b], 564, 1269, 2092 (2023)[c], 3355
$n = 1$	(0.675, 77.12, 77.97)[d]	A″	508
NO ($^2\Pi$),	16.35, 16.35, 0.0	Σ^+	1988 (1904)[e]
n = 1	(16.43, 16.43, 0.0)[e]		
CO ($^1\Sigma^+$),	14.46, 14.46, 0.0	Σ^+	2220 (2170)[e]
$n = 1$	(14.50, 14.50, 0.0)[e]		
CO$_2$ ($^1\Sigma_g^+$),	71.53, 71.53, 0.0	Σ_g^+	1376 (1385)[e]
$n = 2$	(71.50, 71.50, 0.0)[e]	Σ_u^+	2436 (2349)[e]
		Π_u	666 (667)[e]
HCN ($^1\Sigma^+$),	18.73, 18.73, 0.0	Σ^+	2200 (2096)[e], 3456 (3312)[e]
$n = 1$	(18.86, 18.86, 0.0)[e]	Π	787 (714)[e]
HCNO ($^1\Sigma^+$),	72.88, 72.88, 0.0	Σ^+	1301 (1254)[f], 2335 (2196)[f], 3514 (3336)[f]
$n = 1$	(73.22, 73.22, 0.0)[g]	Π	242 (224)[f], 570 (537)[f]

[a] Calculated at the B3LYP/6-311G(d,p) level, experimental values are given in parentheses if available. [b] Reference 42. [c] Reference 13. [d] Reference 38. [e] Reference 53. [f] Reference 75. [g] Reference 76.

TABLE 6: Moments of Inertia, Symmetry Numbers (*n*), and Vibrational Frequencies[a] of the Intermediates and Transition States

species/TS	moments of inertia, I_A, I_B, $I_C/10^{-40}$ g cm^2	vibrational frequencies: symm	vibrational frequencies: ν/cm^{-1}
1, $n = 1$	16.89, 324.83, 341.72	A′	183, 536, 568, 1011, 1096, 1330, 1563, 2233, 3186
		A″	174, 572, 678
2, $n = 1$	57.00, 213.66, 270.66	A′	137, 406, 789, 902, 1127, 1268, 1585, 2211, 3264
		A″	214, 601, 634
3, $n = 1$	53.50, 147.48, 200.98	A′	478, 658, 762, 966, 1057, 1215, 1640, 1969, 3235
		A″	276, 740, 839
3-rad, $n = 2$	65.67, 180.02, 245.69	A′	172, 486, 623, 853, 1112, 1170, 1530, 1706, 3026
		A″	94, 554, 866
TS1, $n = 1$	56.37, 169.76, 226.14	A′	290i, 364, 797, 982, 1169, 1247, 1411, 2137, 3252
		A″	251, 670, 693
TS6, $n = 1$	37.57, 292.84, 313.12	A′	418i, 171, 290, 484, 537, 713, 776, 1070, 1285, 1689, 2223, 3249
TS2, $n = 1$	65.93, 154.18, 220.10	A′	867i, 369, 490, 665, 933, 1171, 1786, 1901, 3178
		A″	148, 669, 827
cis-TS3, $n = 1$	78.01, 162.83, 240.84	A′	475i, 158, 450, 668, 992, 1303, 1927, 2055, 3349
		A″	247, 484, 617
trans-TS3, $n = 1$	43.51, 269.42, 312.93	A′	470i, 116, 339, 733, 1005, 1345, 1826, 2056, 3002
		A″	119, 456, 579
C1-TS3, $n = 1$	52.52, 254.33, 296.91	A′	535i, 170i, 101, 285, 493, 578, 738, 1049, 1306, 1816, 2062, 3297
TS3a, $n = 1$	45.88, 260.25, 306.13	A′	606i, 196, 410, 695, 1134, 1285, 1916, 2089, 3132
		A″	241, 432, 715
TS-rad, $n = 1$	65.02, 163.57, 228.59	A′	212i, 450, 600, 807, 1104, 1127, 1627, 1719, 3090
		A″	158, 608, 870
TS2-rad, $n = 2$	68.84, 172.63, 241.47	A′	1194i, 176, 501, 645, 1121, 1169, 1251, 1723, 3062
		A″	65, 578, 852

[a] Calculated at the B3LYP/6-311G(d,p) level.

decompose to $N_2 + CO_2$. On the other hand, the effects of the overlooked analogues of **TS6** and **cis-TS3** on the total rate constant of the NCO + NO reaction and its product distribution could be nonnegligible and warrant further revision of that system.

Enthalpy of Formation of *trans*-Nitrosoketene. Calculation of the enthalpy for the initial addition (R1t) to form *trans*-nitrosoketene (**1**), at the present highest levels of theory, QCISD(T)/(II) and CCSD(T)/(II), resulted in −44.2 and −44.4 kcal/mol, respectively, whereas previously calculated enthalpies for this channel were −40.0 kcal/mol at the QCISD(T)/6-31G(d,p) level[20] and −41.6 kcal/mol at the CCSD(T)/6-311+G(2df,p) level.[21]

$$\mathrm{HCCO + NO = 1} \qquad \text{(R1t)}$$

Such a discrepancy motivated us to examine the enthalpy of the initial reaction step more carefully. We used an isodesmic reaction[52] (R2) to calculate the heat of formation of intermediate **1** at several correlated levels of theory.

$$\mathbf{1} + \mathrm{C_2H_4} = t\text{-}\mathrm{C_2H_3NO} + \mathrm{CH_2CO} \qquad \text{(R2)}$$

The enthalpy of formation of *trans*-nitrosoketene was derived from the isodesmic reaction analysis as follows:

$$\Delta_f H^\circ_0(\mathbf{1}) = \Delta_f H^\circ_0(t\text{-}\mathrm{C_2H_3(NO)}) + \Delta_f H^\circ_0(\mathrm{CH_2CO}) - \Delta_f H^\circ_0(\mathrm{C_2H_4}) - \Delta H^\circ_{R2}(0\ \mathrm{K}) \quad (1)$$

where the enthalpy of reaction (R2), $\Delta H^\circ_{R2}(0\ \mathrm{K})$, was evaluated theoretically in this work, whereas the enthalpies of formation of *trans*-nitrosoethylene (t-C_2H_3NO), ketene (CH_2CO), and ethylene (C_2H_4) have been established elsewhere[53−55] (see Table 3).

Table 4 lists the predicted values of $\Delta_f H^\circ_0(\mathbf{1})$ and the 0 K enthalpies for the initial addition step, ΔH°_{R1t} (0 K), calculated either using this value and experimental enthalpies of formation for HCCO and NO or directly, i.e., from the differences between the ZPE-corrected electronic energies of HCCO + NO and **1**. The idea of using an isodesmic reaction is to take advantage of an error cancellation because of similar types of atoms and

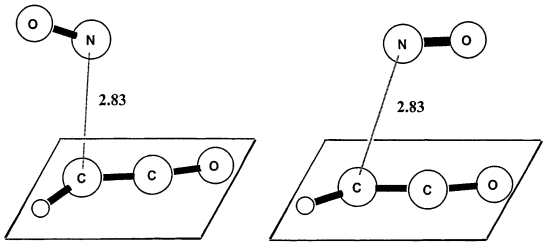

Figure 3. Selected geometries along the minimum energy paths (R(N−O) = 2.83 Å). The addition of NO to the HCCO(^{2}A″) radical occurs perpendicularly to the HCCO plane.

chemical bonds in the compounds on the right- and left-hand sides of such a model reaction. For the present case, there is an additional advantage of an isodesmic reaction approach, because both HCCO and NO have almost degenerate ground electronic states, and therefore, the direct calculation of $\Delta H°_{R1t}(0\ K)$ using single reference methods, especially perturbation theory, may be significantly in error. Clearly, from Table 4, the values of $\Delta H°_{R1t}(0\ K)$ derived based on the isodesmic reaction at different levels of theory are much less scattered than the corresponding values calculated directly. By inspecting the results in Table 4, an estimation of the heat of formation of *trans*-nitrosoketene can be made quite reliably. First of all, we note that the basis set limit is reached with the 6-311+G(3df,2p) ≡ (II) basis set, because the values calculated with 6-311G(2df,p) and (II) do not differ by more than 0.2 kcal/mol for the same method. MPn series ($n = 1-4$) converge; thus, from the difference between the MP3 and MP4 values, we find the lower and upper bounds: $18.2 \le \Delta_f H°_0(\mathbf{1}) \le 20.1$ kcal/mol. The QCISD(T)/(II) and CCSD(T)/(II) results, 18.6 and 18.9 kcal/mol, nicely fit in this interval closer to the MP4 border, as expected for a true limit. Taking the average value as a base and adding an experimental uncertainty of 1.5 + 0.1 + 0.1 kcal/mol (because of combined experimental uncertainties for nitrosoethylene, ethylene, and ketene), one obtains $\Delta_f H°_0(\mathbf{1}) = 18.8 \pm 1.7$ kcal/mol. Corrected to the room temperature, the enthalpy of formation becomes $\Delta_f H°_{298}(\mathbf{1}) = 17.8 \pm 1.7$ kcal/mol.

Hence, from the isodesmic enthalpy of formation of **1** and accurate experimental enthalpies of formation of NO and HCCO radicals (Table 3), the heat of their recombination can be estimated as $\Delta H°_{R1t}(0K) = -44.9 \pm 1.8$ kcal/mol and $\Delta H°_{R1t}(298\ K) = -46.0 \pm 1.8$ kcal/mol. The last column of Table 4 lists the values of $\Delta H°_{R1t}(0K)$ calculated directly by various methods. Among them, the QCISD(T)/(II) and CCSD(T)/(II) predictions are the most accurate, and they are very close to our best recommendation obtained from the isodesmic reaction analysis.

Variational Calculation of the Entrance Transition States. As the initial reaction of HCCO and NO is a barrierless radical−radical association, a variational treatment of the reaction coordinate is required. We computed two separate minimum energy paths (MEPs) for the dissociation of **1** and **2** to HCCO(^{2}A″) + NO by stretching the C−N bond up to 4.5 Å with 0.1 Å increments. For the present calculation, we ignored the excited A′ state of HCCO. Possible errors caused by this approximation will be discussed at the end of this section. Sample structures along the MEPs are illustrated in Figure 3. The A″ state of HCCO has an unpaired electron perpendicular to the molecular plane; therefore, the molecular geometries along the dissociation profiles are nonplanar, although both adducts **1** and **2** have a planar structure. Symmetry removal during the dissociation of **1** and **2** to HCCO(^{2}A″) + NO creates two enantiomeric pathways for each reaction. This will be accounted for in the rate constant calculations by introducing a path degeneracy $l'' = 2$ for the HCCO(^{2}A″) + NO recombination reactions producing either **1** or **2**. The same path degeneracy factors apply to the reverse dissociations.

We should mention that although transient structures along the dissociation profiles are singlet states, unrestricted DFT formalism must be used in the electronic structure calculations because restricted solutions of the Kohn−Sham equations become unstable at long separations (R(C−N) > 2.3 Å). The use of an unrestricted B3LYP functional allowed us to obtain reasonable dissociation profiles with smooth point-to-point variations of the energetic and molecular parameters. The potential energies, ZPEs, moments of inertia, and vibrational frequencies orthogonal to the reaction coordinate for different variational points used in the rate constant calculations are collected in Tables S1 and S2 of the Supporting Information. The canonical variational transition state theory (CVTST) rate constant calculations will be discussed in the next section, where they will be coupled with the RRKM/master equation analysis of the decomposition of the chemically activated nitrosoketene.

As mentioned earlier, HCCO radical possesses a low-lying excited state, ^{2}A′, which results from the Renner-Teller splitting of a doubly degenerate $^2\Pi$ state. Both components can, in principle, react with NO. Possible errors caused by neglecting the excited electronic states of HCCO and of variational transition states can be estimated. For that, let us write down the total path degeneracy combined with electronic degeneracy factors for an entrance channel (to form either **1** or **2**) as

$$G = [l''g''_{TS} + l'g'_{TS}\exp(-\Delta E_{TS}/RT)]/ [g_{HCCO}(^2A'') + g_{HCCO}(^2A')\exp(-\Delta E_{HCCO}/RT)]\, G_{NO} \quad (2)$$

where G_{NO} is the electronic partition function of NO, ΔE_{TS} and ΔE_{HCCO} are the splittings between the ground and the first excited state for a variational transition state and HCCO, and $g''_{TS} = g'_{TS} = 1$ and $g_{HCCO}(^2A'') = g_{HCCO}(^2A') = 2$ are the corresponding electronic degeneracies. This expression also incorporates path degeneracy factors, $l''$and l', for paths originating from HCCO(^{2}A″) and HCCO(^{2}A′), respectively. $l' = 1$, because the recombination of HCCO(^{2}A′) and NO radicals occurs in-plane, whereas the addition to HCCO(^{2}A″) does not preserve the C_s symmetry, and therefore, $l'' = 2$.

Substituting these values into eq 2, one can rewrite it in a more compact form:

$$G = [2 + \exp(-\Delta E_{TS}/RT)]/ [2 + 2\exp(-\Delta E_{HCCO}/RT)]G_{NO} \quad (3)$$

The calculation of the rate constant presented in this paper assumed that both ΔE_{TS} and ΔE_{HCCO} were large enough to neglect the exponential terms, so that $G° = 1/G_{NO}$. Therefore, the calculated rate constant is in error by a factor of $[2 + \exp(-\Delta E_{TS}/RT)]/[2 + 2\exp(-\Delta E_{HCCO}/RT)] = G/G^0$. It is probable that at long separations (which correspond to the VTST locations at low T), $\Delta E_{TS} \approx \Delta E_{HCCO}$, whence

$$G/G^0 \approx [2 + \exp(-\Delta E_{HCCO}/RT)]/ [2 + 2\exp(-\Delta E_{HCCO}/RT)] \le 1 \quad (4)$$

Then, at low temperatures, the rate constant could be overestimated, though only slightly, because at low T, $\exp(-\Delta E_{HCCO}/RT) \approx 0$. For example, the G/G^0 ratio defined by (4) equals 0.977 at 500 K and 0.997 at 300 K assuming $\Delta E_{HCCO} = 3$ kcal/mol.

At high temperatures, VTST locations shift to shorter separations, where ΔE_{TS} should be smaller than ΔE_{HCCO}. In the limiting case that $\Delta E_{TS} \rightarrow 0$

$$G/G^0 \rightarrow 3/[2 + 2\exp(-\Delta E_{HCCO}/RT)] \qquad (5)$$

eq 5 gives $G/G^0 = 1.23$ at 1000 K, which decreases to less than unity at $T > 2000$ K and can drop as low as 3/4 when T is raised to infinity. In the opposite limit that $\Delta E_{TS} \approx \Delta E_{HCCO}$, eq 4 will apply, suggesting the total rate is overestimated by 9% at 1000 K and 18% at 2500 K.

Thus, we can conclude that the errors introduced as a result of neglecting the $^2A'$ state of HCCO are negligible at low T (primarily because of low occupancy of this state) and amount to less than 25% at high T, as follows from equations (4) and (5).

Multichannel Variational RRKM Calculations. On the basis of theoretical energetic and molecular parameters of the reactants, products, intermediates, and transition states, the rate constant calculations were carried out with a recently updated version 1.19 (Feb. 20, 2002) of the ChemRate program[56] from NIST. We used a weak collision master equation/RRKM modeling with a variational treatment of the entrance channels to derive effective rate constants and product distribution according to the *virtual component* formalism of Knyazev and Tsang.[57]

Because variational calculations are currently not supported in the ChemRate program, the canonical variational TST (CVTST) calculations for the HCCO + NO recombination channels were performed externally with the POLYRATE program,[58] using the electronic structure input files which contained energies, gradients, and force constants at selected points on the reaction paths (~20 points for each channel). These points were selected from the interval that covers the effective locations of variational transition states at $T = 250-2500$ K (R(C−N) = 2.0−3.7 Å for HCCO + NO → **1**; R(C−N) = 2.0−4.3 Å for HCCO + NO → **2)**. The energetic and molecular parameters of these points are available in the Supporting Information (Tables S1 and S2). The MEP quantities for additional points on a fine grid (0.001 Å) were defined from the input (sparse) grid points by n-point ($n = 3, 5$) Lagrange interpolation. The results were stable with respect to the variation of n.

Within the CVTST approximation, the location of variational transition states was determined by maximizing the free energy of activation with respect to reaction coordinate at any given temperature, whence T-dependent molecular and energetic parameters for variational transition states were supplied to the ChemRate program. Then, the interplay of recombination, isomerization, decomposition, and stabilization channels was analyzed by solving the one-dimensional (E-resolved) master equation,[59] which describes the evolution of all active components. Microscopic rate constants $k(E)$ for isomerization and decomposition channels were calculated by RRKM theory.[59−61] In the present study, the energy increment was fixed at 10 cm^{-1} in all sum and density of states calculations, which were performed using the modified Beyer−Swinehart algorithm.[62] The standard form of the "exponential-down" model[59,63] was used for collisional energy transfer. The frequency of collisions with the bath gas was estimated from the Lennard-Jones parameters adopted from refs 64 and 65, assuming that ϵ/k_B(HC(CO)NO) ≈ ϵ/k_B(HCNO) = 258 K, and σ(HC(CO)NO) ≈ σ(HCNO) = 4.42 Å. The master equation was solved in a matrix form with a method based on the Householder's tridiagonalization algorithm.[66] The energy bin size $\delta E = 100$ cm^{-1} was used in the master equation computations; the matrix size was up to 1500 × 1500 to ensure the convergence at high T. More details about the implementation of the time-dependent master equation/RRKM analysis in ChemRate are available from a series of publications by Tsang and co-workers.[57,67−69]

SCHEME 1

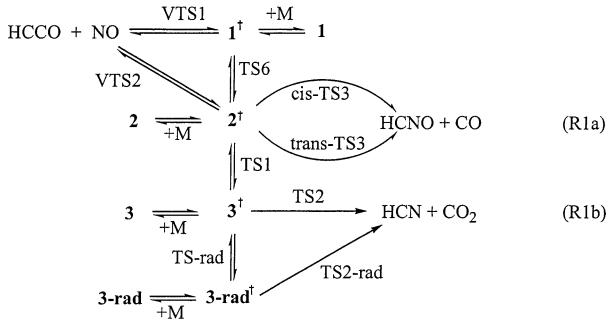

The updated mechanism of reaction R1 can be expressed in Scheme 1. Here, "†" denotes internal excitation, and M represents the third-body (bath gas). The scheme comprises four coupled wells, two variational entrance, and two major product channels. The molecular parameters of the reactants, intermediates, and transition states used in the RRKM/ME calculations are given in Tables 5 and 6. The energetics are defined in Figure 1.

Our kinetic model may at first glance appear rather complex. However, the topology of the PES permits a very straightforward description of the mechanism. We would like to point out that all decomposition pathways lie well below the energy level of the reactants. As a result, the stabilization of all chemically activated intermediates is negligible under a wide range of experimental conditions ($P < 10^5$ Torr, $T = 250-2500$ K), and the reaction proceeds in the steady-state regime. Both effective total and branching rate constants are well-defined and essentially independent of pressure.

The mechanistic details can be summarized as follows. At all T, recombination of HCCO and NO radicals preferably yields **1**†. The selectivity is particularly high at low T. Initially formed **1**† can either isomerize to **2**† or dissociate back to the reactants. The latter process is negligible at low T but consumes a larger fraction of **1**† as the T increases. As a consequence, the effective total rate shows negative T dependence. Only a minor fraction of **2**† returns to the reactants. Instead, **2**† either decomposes to HCNO + CO (R1a) or isomerizes to **3**†. At low T, the CO-extrusion pathway via **cis-TS3** is dominant; however, the cis and trans channels make comparable contributions to the rate of CO production at high T. A small fraction of **3**† can isomerize back to **2**† and then decompose to HCNO + CO. The rest of **3**† produces HCN + CO_2 either via concerted **TS2** or by a stepwise mechanism via **TS-rad**, diradical intermediate **3-rad**, and **TS2-rad**. The first ring-opening step is rate controlling in the latter sequence. Although **TS-rad** lies ~9 kcal/mol higher than **TS2**, the contribution of the diradical branch to the CO_2 production is not negligible and accounts for as much as 15% of the total yield at high T.

The results of our calculations are plotted in Figures 4 and 5 for the temperature range from 250 to 2500 K. In Figure 4, we plotted the effective total rate constant, which is best expressed in the following form: $k_{R1}(T) = 1.37 \times 10^{16}\ T^{-0.98} \exp(-190\text{K}/T)$ $cm^3\ s^{-1}\ mol^{-1}$. It shows an excellent agreement with the room-temperature value of Unfried et al.[13] and recent most extensive experimental set of data by Carl et al.[15] combined

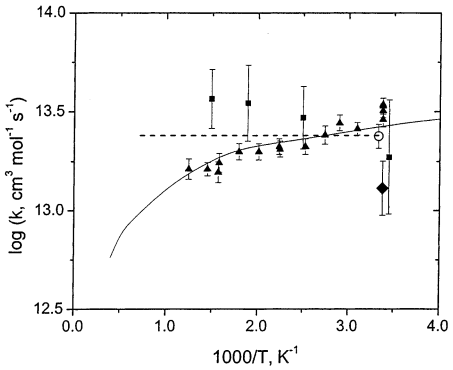

Figure 4. Plot of the effective total rate constant for HCCO + NO in comparison with experimental data. Solid line: this work ($P = 0.1-1000$ Torr); dashed line: Miller et al.;[9] experimental data: circle, Unfried et al.;[13] diamond, Temps et al.;[14] squares, Boullart et al.;[5] triangles, Carl et al.[15]

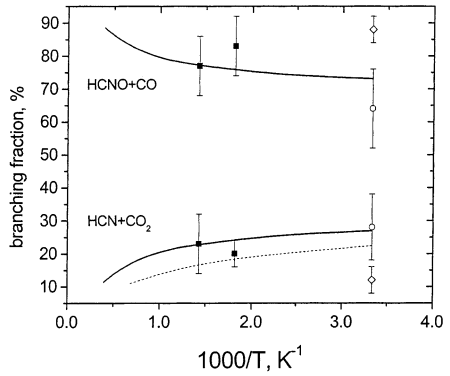

Figure 5. Branching fractions of the two main product channels: HCNO + CO (R1a) and HCN + CO_2 (R1b). Theoretical results: solid line, this work; dashed line, Vereecken et al.[21] Experimental data: squares, Peeters et al.;[5,16] circles, Eickhoff and Temps;[17] diamonds, Rim and Hershberger.[18]

with the earlier measurement by the same group. The rate constant of Temps et al.[14] is lower than our prediction by a factor of 2.

In Figure 5, the calculated and experimental branching fractions of the two main product channels are given. The branching fraction of the HCN + CO_2 channel can be fitted by a double-exponential decay formula: $\alpha = 0.5\exp(-T/67.1) + 0.3\exp(-T/2592)$. Our estimates are in excellent agreement with room-temperature branching fractions of Eickhoff and Temps[17] and within the error limits of high T data of Peeters et al.[5,16] The room-temperature yield of CO_2 reported by Rim and Hershberger[18] is lower by a factor of 2. These authors analyzed the yields of CO and CO_2 from the 193 nm excimer laser photolysis of ketene in the presence of excess amounts of NO. Under these conditions, several initial photolytic products can be formed[70]

$$H_2CCO + h\nu \rightarrow {}^3CH_2 + CO \quad \text{(R3a)}$$

$$\rightarrow {}^1CH_2 + CO \quad \text{(R3b)}$$

$$\rightarrow HCCO + H \quad \text{(R3c)}$$

$$\rightarrow CCO + H_2 \quad \text{(R3d)}$$

Rim and Hershberger assumed that only reactions (R3a), (R3b), and (R1a) need to be considered as CO-producing channels; reaction (R1b) was considered as the source of CO_2 along with the static CO_2 impurity in ketene. Very recently, Eschenko et al.[19] investigated the formation of HCNO and HCN in the same system. They concluded that reactions of CH_2 (both singlet and triplet) with NO, along with (R1a) and (R1b), yield significant amounts of HCNO and HCN via reactions (R4a) and (R4b):

$$CH_2 + NO \rightarrow HCNO + H \quad \text{(R4a)}$$

$$\rightarrow HCN + OH \quad \text{(R4b)}$$

channel (R4a) being the dominant one. The H atoms produced in (R4a) and (R3c) are consumed mainly in the reaction with H_2CCO

$$H + H_2CCO \rightarrow CH_3 + CO \quad \text{(R5)}$$

which could be responsible for a fraction of CO measured by Rim and Hershberger. We should note that the product yields of HCNO and HCN reported by Eschenko et al.[19] can be accounted for with our predicted product branching for the HCCO + NO reaction, $\alpha(298\text{ K}) = k_{1b}/k_1 = 0.27$, when it is combined with known photodissociation yields[70] (R3a−R3d) and the product branching for reaction (R4), $k_{4a}/k_4 = 0.89 \pm 0.06$.[71,72]

Previously, Miller et al.[9] and recently Vereecken et al.[21] attempted to theoretically predict the product branching distribution based on the PES of Nguyen et al.[20] (or its slightly refined version). Because of the incompleteness of PES, Miller et al.[9] were unable to account for the experimentally observed branching fractions, overestimating significantly the fraction of HCN + CO_2 produced. The kinetic model used by Vereecken et al.[21] did not include the major CO-producing pathway (via **cis-TS3**) either. However, they assumed that **trans-TS3** directly connects both **1** and **2** to the HCNO + CO and treated the torsional motion of CO in **trans-TS3** as a free rotor. We found no support for either assumption, but these assumptions effectively compensated the lack of a major CO-producing pathway in the analysis of Vereecken and co-workers. Fortuitously, their product branching is very close (within 10%) to the values estimated in this study based on the complete PES.

To complete the study, we tested the sensitivity of our predicted branching fractions to small variations in the most critical energetic parameters. A variation of ±2 kcal/mol in the energy of **TS1** propagates into the ±0.06 variation in the yield of CO_2 at room temperature, $\alpha(298\text{ K}) = 0.27\pm0.06$. The product branching is less sensitive to the energy of **TS2**. Its shift by ±2 kcal/mol varies $\alpha(298\text{ K})$ by less than ±0.03. Considering an uncertainty of ±2 kcal/mol in the energies of **TS3** (cis and trans), the following error limits of α (CO_2 branching) were derived: $0.18 < \alpha(298\text{ K}) < 0.38$. Finally, a calculation based on the B3LYP/(I) energies for the diradical branch (Table 2) instead of those given in Figure 1 predicts that a higher fraction of HCN + CO_2 will be formed via this branch (16% instead of 7% at room T). At the same time, the total CO_2 yield (α) increases insignificantly (by less than 0.01 at room temperature) and the concerted pathway of the 1,2-oxazet-4-one (**3**) decomposition remains dominant.

Concluding Remarks

As we mentioned earlier, the mechanism of the HCCO + NO reaction is relevant to large-scale modeling of NO_x reduction by reburning technologies. This study provides two key kinetic parameters that determine the importance of HCCO as a recycling agent for NO, namely, the total rate constant and product branching. Previously, Miller et al.[9] recommended temperature-independent value of $k_{R1} = 2.4 \times 10^{13}$ cm^3 mol^{-1}

s^{-1} and a constant value of $\alpha = 0.65$ for kinetic modeling of NO reburning. On the basis of the early kinetic measurements of Peeters et al.,[5,16] temperature-dependent parameters were derived and employed for jet-stirred reactor modeling by Dagaut et al.[11] Both k_{R1} and α had a slightly positive temperature dependence, so that at T above 1000 K, the total rate constant was 4.3×10^{13} cm^3 s^{-1} mol^{-1} and higher, whereas the branching fraction for channel (R1b) exceeded 0.28. Our results suggest that both parameters were overestimated. The total rate constant for reaction (R1), $k_{R1}(T) = 1.37 \times 10^{16}\ T^{-0.98}\ \exp(-190\text{K}/T)$ cm^3 s^{-1} mol^{-1} for $T = 250-2500$ K, slowly decreases with T and falls below 1.3×10^{13} cm^3 mol^{-1} s^{-1} at $T > 1000$ K. Our recommended branching function, $\alpha = 0.5\ \exp(-T/67.1) + 0.3\ \exp(-T/2592)$ for $T = 250-2500$ K, also exhibits negative temperature dependence and falls below 0.2 at $T > 1000$ K. On the basis of the sensitivity of α to changes in the most critical reaction barriers, we can tentatively assign an uncertainty of ± 0.1 to the above theoretical estimate. Therefore, the previously assumed value of $\alpha = 0.65$[9] cannot be confirmed.

In conclusion, our theoretical findings somewhat diminish the role played by the ketenyl radical in the mechanism of NO reburning. This conclusion, however, critically depends on the fate of fulminic acid under combustion conditions. Current models predict that it is rapidly oxidized by OH and O. If alternative secondary reactions of HCNO, such as bimolecular reactions with H and small hydrocarbon radicals, or unimolecular decomposition to HCN + O(^{3}P), or isomerization to HOCN followed by its decomposition to NCO + H,[73] could compete with oxidation channels, then the HCNO + CO branch would also aid to NO reduction. In fact, recent kinetic modeling[11] suggests that the concentration of NO becomes very sensitive to the HCNO + H → HCN + OH reaction under fuel-rich conditions. Questions regarding the secondary chemistry of HCNO and the capacity of species other than HCCO to act as NO-recycling agents still need to be answered in order to create a comprehensive mechanism of NO_x removal by reburning.

Acknowledgment. The authors are grateful for the support of this work in part from the Department of Energy, Office of Basic Energy Sciences, Division of Chemical Sciences through Contract DE-FGO2-97ER14784 to L.V.M. and I.V.T. and in part from the Office of Naval Research to D.V.P. and M.C.L. under Contract N00014-89-J 1949, Dr. J. Goldwasser program manager. Our special thanks goes to Prof. J. Peeters of the University of Leuven for providing us his preliminary data and to the authors of the ChemRate program, in particular to Vladimir Mokrushin and Vadim Knyazev, for enriching discussions and live updates of this software package. Also, we are thankful to the Cherry L. Emerson Center of Emory University for the use of its resources, which is in part supported by a National Science Foundation grant (CHE-0079627) and an IBM Shared University Research Award.

Supporting Information Available: Tables S1 and S2 contain the energetic and molecular parameters of selected points along the HCCO+ NO → **1** and **2** recombination profiles. This material is available free of charge via the Internet at http://pubs.acs.org.

References and Notes

(1) Wendt, J. O.; Sterling, C. V.; Matovich, M. A. *Proc. Combust. Inst.* **1973**, *14*, 897−904.

(2) Chen, S. L.; McCarthy, J. M.; Clark, W. D.; Heap, M. P.; Seeker, W. R.; Pershing, D. W. *Proc. Combust. Inst.* **1986**, *21*, 1159−1169.

(3) Glarborg, P.; Karll, B.; Pratapas, J. M. *Proceedings of the 19th World Gas Conference*; Milano, Italy, 1994 and references therein.

(4) Lissianski, V. V.; Ho, L.; Maly, P. M.; Pizeq, G.; Zamansky, V. M. *Proc. Combust. Inst.* **2002**, *29*, WIP Abstract 1−25−1432.

(5) Boullart, W.; Nguyen, M. T.; Peeters, J. *J. Phys. Chem.* **1994**, *98*, 8036−8043.

(6) Stapf, D.; Lueckel, W. *Proc. Combust. Inst.* **1996**, *26*, 2083.

(7) Glarborg, P.; Alzueta, M. U.; Dam-Johansen, K.; Miller, J. A. *Combust. Flame* **1998**, *115*, 1−27.

(8) Prada, L.; Miller, J. A. *Combust. Sci. Tech.* **1998**, *132*, 225−250.

(9) Miller J. A.; Durant, J. L.; Glarborg, P. *Proc. Combust. Inst.* **1998**, *27*, 235−243.

(10) Dagaut, P.; Lecomte, F.; Chevailler, S.; Cathonnet, M. *Combust. Sci. Technol.* **1998**, *139*, 329−363.

(11) Dagaut, P.; Luche, J.; Cathonnet, M. *Int. J. Chem. Kinet.* **2000**, *32*, 365−377.

(12) Dagaut, P.; Luche, J.; Cathonnet, M. *Fuel* **2001**, *80*, 979−986, and references therein.

(13) Unfried, K. G.; Glass, G. P.; Curl, R. F. *Chem. Phys. Lett.* **1991**, *177*, 33−38.

(14) Temps, F.; Wagner, H. Gg.; Wolf, M. *Z. Phys. Chem.* **1992**, *176*, 27−39.

(15) Carl, S. A.; Sun, Q.; Vereecken, L.; Peeters, J. HCCO + NO rate measurements. *J. Phys. Chem. A* **2002**, *106*, 12242.

(16) Van Poppel, M.; Peeters, J. *Proceedings of the 15th International Symposium on Gas Kinetics*; Bilbao, Spain, 1998; pp 147−148.

(17) Eickhoff, U.; Temps, F. *Phys. Chem. Chem. Phys.* **1999**, *1*, 243−251.

(18) Rim, K. T.; Hershberger, J. F. *J. Phys. Chem. A* **2000**, *104*, 293−296.

(19) Eshchenko, G.; Kocher, T.; Kerst, C.; Temps, F. *Chem. Phys. Lett.* **2002**, *356*, 181−187.

(20) Nguyen, M. T.; Boulart, W.; Peeters, J. *J. Phys. Chem.* **1994**, *98*, 8030−8035.

(21) Vereecken, L.; Sumathy, R.; Carl, S. A.; Peeters, J. *Chem. Phys. Lett.* **2001**, *344*, 400−406.

(22) Frisch, M. J.; Trucks, G. W.; Schlegel, H. B.; Scuseria, G. E.; Robb, M. A.; Cheeseman, J. R.; Zakrzewski, V. G.; Montgomery, J. A., Jr.; Stratmann, R. E.; Burant, J. C.; Dapprich, S.; Millam, J. M.; Daniels, A. D.; Kudin, K. N.; Strain, M. C.; Farkas, O.; Tomasi, J.; Barone, V.; Cossi, M.; Cammi, R.; Mennucci, B.; Pomelli, C.; Adamo, C.; Clifford, S.; Ochterski, J.; Petersson, G. A.; Ayala, P. Y.; Cui, Q.; Morokuma, K.; Malick, D. K.; Rabuck, A. D.; Raghavachari, K.; Foresman, J. B.; Cioslowski, J.; Ortiz, J. V.; Stefanov, B. B.; Liu, G.; Liashenko, A.; Piskorz, P.; Komaromi, I.; Gomperts, R.; Martin, R. L.; Fox, D. J.; Keith, T.; Al-Laham, M. A.; Peng, C. Y.; Nanayakkara, A.; Gonzalez, C.; Challacombe, M.; Gill, P. M. W.; Johnson, B. G.; Chen, W.; Wong, M. W.; Andres, J. L.; Head-Gordon, M.; Replogle, E. S.; Pople, J. A. *Gaussian 98*, revision A.7; Gaussian, Inc.: Pittsburgh, PA, 1998.

(23) (a) Becke, A. D. *J. Chem. Phys.* **1993**, *98*, 5648. (b) Becke, A. D. *Phys. Rev. A* **1988**, *38*, 3098.

(24) (a) Lee, C.; Yang, W.; Parr, R. G. *Phys. Rev. B* **1988**, *37*, 785. (b) Stephens, P. J.; Devlin, F. J.; Chabalowski, C. F.; Frisch, M. J. *J. Phys. Chem.* **1994**, *98*, 11623.

(25) (a) Gonzalez, C.; Schlegel, H. B. *J. Chem. Phys.* **1989**, *90*, 2154−2161. (b) Gonzalez, C.; Schlegel, H. B. *J. Phys. Chem.* **1990**, *94*, 5523−5527.

(26) The performance of the B3LYP functional for geometry optimization was assessed, for example, by the authors of several versatile model chemistries: G2(B3LYP/MP2/CC) (Bauschlicher, C. W.; Partridge, H. *J. Chem. Phys.* **1995**, *103*, 1788−1791), G2M (Mebel, A. M.; Morokuma, K.; Lin, M. C. *J. Chem. Phys.* **1995**, *103*, 7414−7421), G3//B3LYP (Baboul, A. G.; Curtiss, L. A.; Redfern, P. C.; Raghavachari, K. *J. Chem. Phys.* **1999**, *110*, 7650−7657), and G3X (Curtiss, L. A.; Redfern, P. C.; Raghavachari, K.; Pople, J. A. *J. Chem. Phys.* **2001**, *114*, 108−117).

(27) Wittbrodt, J. M.; Schlegel, H. B. *J. Chem. Phys.* **1996**, *105*, 6574−6577.

(28) Harding, L. B. *J. Phys. Chem.* **1981**, *85*, 10−11.

(29) Harding, L. B.; Wagner, A. F. *J. Phys. Chem.* **1986**, *90*, 2974.

(30) Goddard, J. D. *Chem. Phys. Lett.* **1989**, *154*, 387−390.

(31) Szalay, P. G.; Stanton, J. F.; Bartlett, R. J. *Chem. Phys. Lett.* **1992**, *193*, 573−579.

(32) Hu, C. H.; Schaefer, H. F.; Hou, Z.; Bayes, K. D. *J. Am. Chem. Soc.* **1993**, *115*, 6904.

(33) Szalay, P. G.; Fogarasi, G.; Nemes, L. *Chem. Phys. Lett.* **1996**, *263*, 91−99.

(34) Schäfer, B.; Perić, M.; Engels, B. *J. Chem. Phys.* **1999**, *110*, 7802−7810.

(35) Yarkony, D. *J. Phys. Chem.* **1996**, *100*, 17439−17445.

(36) Szalay, P. G.; Blaudeau, J. P. *J. Chem. Phys.* **1997**, *106*, 436−437.

(37) Mordaunt, D. H.; Osborn, D. L.; Choi, H.; Bise, R. T.; Neumark, D. M. *J. Chem. Phys.* **1996**, *105*, 6078−6081.

(38) Endo, Y.; Hirota, E. *J. Chem. Phys*. **1987**, *86*, 4319−4326.
(39) Ohsima, Y.; Endo, Y. *J. Mol. Spectrosc*. **1993**, *159*, 458−467.
(40) Jacox, M. E.; Olson, W. B. *J. Chem. Phys.* **1987**, *86*, 3134.
(41) Unfried, K. G.; Curl, R. F. *J. Mol. Spectrosc*. **1991**, *150*, 86.
(42) Brock, L. R.; Mischler, B.; Rohlfing, E. A.; Bise, R. T.; Neumark, D. M. *J. Chem. Phys.* **1997**, *107*, 665−668.
(43) Osborn, D. L.; Mordaunt, D. H.; Choi, H.; Bise, R. T.; Neumark, D. M. *J. Chem. Phys*. **1997**, *106*, 10087−10098.
(44) Badawi, H. M.; Forner, W. *J. Mol. Structure (THEOCHEM)* **2001**, *542*, 7−20.
(45) Woodward, R. B.; Hoffman, R. *J. Am. Chem. Soc*. **1965**, *87*, 395.
(46) Wang, S. G.; Schwarz, W. H. *J. Chem. Phys*. **1996**, *105*, 4641.
(47) (a) Beno, B. R.; Fennen, J.; Houk, K. N.; Lindner, H. J.; Hafner, K. *J. Am. Chem. Soc*. **1998**, *120*, 10490. (b) Haller, J.; Beno, B. R.; Houk, K. N. *J. Am. Chem. Soc*. **1998**, *120*, 6468. (c) Goldstein, Beno, B. R.; Houk, K. N. *J. Am. Chem. Soc*. **1996**, *118*, 6036.
(48) Garavelli, M.; Bernardi, F.; Olivucci, M.; Robb, M. *J. Am. Chem. Soc*. **1998**, *120*, 10210.
(49) (a) Goddard, J. D.; Chen, X.; Orlova, G. *J. Phys. Chem. A* **1999**, *103*, 4078. (b) Goddard, J. D.; Orlova, G. *J. Chem. Phys*. **1999**, *111*, 7705.
(50) Zhu, R.; Lin, M. C. *J. Phys. Chem. A* **2000**, *104*, 10807−10811.
(51) Perry, R. A.; Siebers, D. L. *Nature (London)* **1986**, *342*, 657−658.
(52) Hehre, W. J.; Radom, L.; Schleyer, P. v. R.; Pople, J. A. *Ab initio Molecular Orbital Theory*; John Wiley & Sons: New York, 1986.
(53) Chase, M. W., Jr. NIST-JANAF Thermochemical Tables, 4th ed.; *J. Phys. Chem. Ref. Data* **1998**, Monograph No. 9.
(54) Luo, Yu Ran; Holmes, J. L. *J. Phys. Chem.* **1992**, *96*, 9568−9571.
(55) Traeger, J. C. *Int. J. Mass Spectrom*. **2000**, *194*, 261−267.
(56) Mokrushin, V.; Bedanov, V.; Tsang, W.; Zachariah, M.; Knyazev, V. ChemRate, version 1.19; NIST: Gaithersburg, MD, 2002.
(57) Knyazev, V. D.; Tsang, W. *J. Phys. Chem. A* **1999**, *103*, 3944−3954.
(58) Corchado, J. C.; Chuang, Y.-Y.; Fast, P. L.; Villa, J.; Hu, W.-P.; Liu, Y.-P.; Lynch, G. C.; Nguyen, K. A.; Jackels, C. F.; Melissas, V. S.; Lynch, B. J.; Rossi, I.; Coitino, E. L.; Ramos, A. F.; Steckler, R.; Garrett, B. C.; Isaacson, A. D.; Truhlar, D. G. POLYRATE, version 8.5.1; Department of Chemistry and Supercomputer Institute: University of Minnesota, Minneapolis, MN, 2000.
(59) Gilbert, R. G.; Smith, S. C. *Theory of Unimolecular and Recombination Reactions*; Blackwell Scientific Publications: Oxford, 1990.
(60) Forst, W. *Theory of Unimolecular Reactions*; Academic Press: New York, 1973.
(61) Robinson, P. J.; Holbrook, K. A. *Unimolecular Reactions*; Wiley: New York, 1972.
(62) Astholz, D. C.; Troe, J.; Wieters, W. *J. Chem. Phys*. **1979**, *70*, 5107.
(63) Rabinovitch, B. S.; Tardy, D. C. *J. Chem. Phys*. **1966**, *45*, 3720.
(64) Reid, R.; Sherwood, T. K. *The properties of gases and liquids*; McGraw-Hill: New York, 1969.
(65) Marchand, N.; Rayez, J. C.; Smith, S. C. *J. Phys. Chem. A* **1998**, *162*, 3358.
(66) Wilkinson, J. H.; Reinsch, C. *Linear Algebra*; Springer: New York, 1971.
(67) Tsang, W.; Bedanov, V.; Zachariah, M. R. *J. Phys. Chem*. **1996**, *100*, 4011.
(68) Bedanov, V. M.; Tsang, W.; Zachariah, M. R. *J. Phys. Chem*. **1995**, *99*, 11452.
(69) Knyazev, V. D.; Tsang, W. *J. Phys. Chem. A* **2000**, *104*, 10747−10765.
(70) Glass, G. P.; Kumaran, S. S.; Michael, J. V. *J. Phys. Chem. A* **2000**, *104*, 8360.
(71) Grubdorf, J.; Temps, F.; Wagner, H. Gg. *Ber. Bunsen-Ges. Phys. Chem*. **1997**, *101*, 134.
(72) Fikri, M.; Meyer, St.; Roggenbuck, J.; Temps, F. *Faraday Disc*. **2001**, *119*, 223.
(73) Mebel, A. M.; Luna, A.; Lin, M. C.; Morokuma, K. *J. Chem. Phys*. **1996**, *105*, 6439−6454.
(74) East, A. L. L.; Allen, W. D. *J. Chem. Phys*. **1993**, *99*, 4638−4650. East, A. L. L.; Johnson, C. S.; Allen, W. D. *J. Chem. Phys*. **1993**, *98*, 1299−1328.
(75) Albert, S.; Winnewisser, M.; Winnewisser, B. P. *Ber. Bunsen-Ges. Phys. Chem*. **1996**, *100*, 1876.
(76) Winnewisser, M.; Winnewisser, B. P. *Z. Naturforsch*. **1971**, *A26*, 128−131.